Progress In Electromagnetics Research M, Vol. 30, 117–128, 2013

MULTI-OUTPUT LEAST SQUARE SUPPORT VECTOR MACHINE FOR THE RECONSTRUCTION OF PERFECT ELECTRIC CONDUCTOR BELOW ROUGH SURFACE

Jiliang Cai[1, *], Chuangming Tong[1, 2], and Weijie Ji[1]

[1]Missile Institute, Air Force Engineering University, Xi'an, Shanxi 710051, China

[2]State Key Laboratory of Millimeter Wave, Nanjing, Jiangsu 210096, China

Abstract—To save the computation time and improve the accuracy of reconstruction results by support vector machine (SVM), a multi-output least square SVM (LS-SVM) algorithm is proposed to reconstruct the position of a 2-D perfect electric conductor (PEC) cylinder below a rough surface. Firstly, the scattered electromagnetic field at a number of observation positions is calculated by the method of moment to generate the training and testing data. Then the multi-output LS-SVM is trained to reconstruct the coordinate of the object center. Numerical results show that this approach is accurate and efficient even with some additive Gaussian noise.

1. INTRODUCTION

More and more attention has been drawn to the reconstruction of the target below the surface, since it has a wide potential use in military and civilian applications, such as remote sensing, ground penetrating radar, non-destructive evaluation. Generally speaking, either the land surface or sea surface can be categorized into two types: One is planer surface [1, 2], and the other is rough surface [3–5]. Compared with the former one, the rough surface is more common in real applications. But the reconstruction of the target below the rough surface has not been as extensively researched as the reconstruction of the target below the planer surface.

Usually, the reconstruction of target below rough surfaces can be cast into an inverse electromagnetic scattering problem and solved by

Received 15 December 2012, Accepted 8 April 2013, Scheduled 12 April 2013

* Corresponding author: Jiliang Cai (shitouji840716@126.com).

different methods. In [5], the reconstruction is posed as a nonlinear least-squares optimization problem, which is solved by Levenberg-Marquardt iterative algorithm. Paper [6] also views the reconstruction as a optimization problem, but it is solved by a modified particle swarm optimization algorithm. In [7], a two-step procedure for characterizing obstacles under a rough surface is proposed. In [8], a Green function for the rough surface is proposed, and the Tikhonov regularization method is used for the imaging of dielectric target buried below rough surface. However, when real-time or quasi real time performance is required, these approaches may become impracticable because of high computation cost.

In fact, there are circumstances when only an estimate of some object properties (e.g., scatters presence or absence) with amount of a-priori information about the problem is required. In such circumstances, artificial neural network (ANN) views the reconstruction as a regression problem and solves it using learning by examples approach. Once trained properly, they can reconstruct the unknowns within a second. In [1], multi-layered perceptron ANN (MLPANN) is used in the detection of dielectric cylinders buried in a lossy half space. However, inherent drawbacks, such as being trapped into local minimal and over fitting, have limited its further application. Support vector machine (SVM) [9], another learning by example method, can avoid these shortcomings of ANN by solving a constrained quadratic optimization problem during the training process and thus achieve more precise reconstruction results [10–14].

Unlike ANNS' multi-input and multi-output mapping ability, in most of the reconstruction occasions, SVM is used as multi-input and single-output mode [10–14], i.e., one SVM corresponds to only one parameter. When there are more parameters to be reconstructed, more irrelevant models need to be established and trained. But this is time-consuming. Moreover, the interactions among different outputs may be neglected, which means that the reconstruction results may not be very accurate. To overcome these drawbacks, in [15] multi-output LS-SVM is proposed to deal with the dielectric cylinder reconstruction in free space. In this paper, it is used to the detection of 2-D perfect dielectric conductor (PEC) target below rough surface.

The remainder of this paper is organized as follows. In Section 2, forward scattering problem of a PEC target below rough surface is described, and in Section 3, inverse scattering problem is formulated by the regression method. The multi-output LS-SVM is briefly introduced in Section 4. In Section 5, the reconstruction results are shown and discussed. Section 6 gives conclusions of this paper.

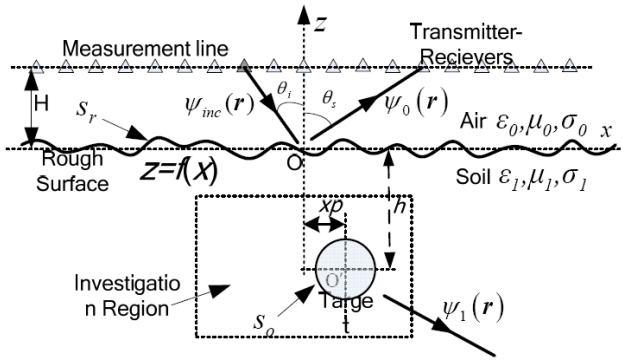

Figure 1. Geometric configuration of the 2-D scattering problem.

2. FORWARD PROBLEM

The geometric configuration of the 2-D scattering problem is shown in Fig. 1. A two-dimensional infinite long circular PEC target with its axis paralleling to the y-axis is buried at the height of h below the rough interface between the air and the lossy earth ground. The upper half space is the free space with the dielectric permittivity ϵ_0, permeability μ_0 and conductivity σ_0. The lower half space is the lossy earth ground with the dielectric permittivity ϵ_1 permeability μ_1 and conductivity σ_1. The receivers are equally distributed on the measurement line above the rough surface at H. A TM polarized tapered wave $\Psi_{inc}(\mathbf{r})$ from the transmitter illuminates the ground with an incident angle θ_i. The receivers receive the scattered field at θ_s. Suppose that Ψ_0 and Ψ_1 are the wave function in the air and ground, respectively. They follow the following integral equations:

$$\frac{1}{2}\Psi_0(\mathbf{r})=\int_{S_r}\left[\Psi_0(\mathbf{r}')\frac{\partial G_0(\mathbf{r},\mathbf{r}')}{\partial \mathbf{n}'}-G_0(\mathbf{r},\mathbf{r}')\frac{\partial \Psi_0(\mathbf{r}')}{\partial \mathbf{n}'}\right]ds'+\Psi_{inc}(\mathbf{r})\ \mathbf{r}\in S_r \quad (1a)$$

$$\frac{1}{2}\Psi_1(\mathbf{r})=-\int_{S_r}\left[\Psi_1(\mathbf{r}')\frac{\partial G_1(\mathbf{r},\mathbf{r}')}{\partial \mathbf{n}'}-G_1(\mathbf{r},\mathbf{r}')\frac{\partial \Psi_1(\mathbf{r}')}{\partial \mathbf{n}'}\right]ds' - \int_{S_o}\left[\Psi_1(\mathbf{r}')\frac{\partial G_1(\mathbf{r},\mathbf{r}')}{\partial \mathbf{n}'}\right]ds' \quad \mathbf{r}\in S_r \quad (1b)$$

$$\frac{1}{2}\Psi_1(\mathbf{r})=-\int_{S_r}\left[\Psi_1(\mathbf{r}')\frac{\partial G_1(\mathbf{r},\mathbf{r}')}{\partial \mathbf{n}'}-G_1(\mathbf{r},\mathbf{r}')\frac{\partial \Psi_1(\mathbf{r}')}{\partial \mathbf{n}'}\right]ds' - \int_{S_o}\left[\Psi_1(\mathbf{r}')\frac{\partial G_1(\mathbf{r},\mathbf{r}')}{\partial \mathbf{n}'}\right]ds' \quad \mathbf{r}\in S_o \quad (1c)$$

where S_r represents the rough surface and S_o the surface of the target. $G_{0,1}(\mathbf{r},\mathbf{r}') = (j/4)H_0^{(1)}(k_{0,1}\,|\mathbf{r}-\mathbf{r}'|)$ are the Green functions in the air and earth, respectively. $H_0^{(1)}(\cdot)$ is zeroth-order Hankel function of the first kind. $\mathbf{r}$ and $\mathbf{r}'$ represent the field point and source point, respectively.

The boundary condition is as:

$$\Psi_0(\mathbf{r})\,|_{\mathbf{r}\in S_r} = \Psi_1(\mathbf{r})\,|_{\mathbf{r}\in S_r} \tag{2a}$$

$$\frac{\partial\Psi_0(\mathbf{r})}{\partial\mathbf{n}}|_{\mathbf{r}\in S_r} = \frac{1}{\rho}\frac{\partial\Psi_1(\mathbf{r})}{\partial\mathbf{n}}|_{\mathbf{r}\in S_r} \quad \rho=\epsilon_1/\epsilon_0 \tag{2b}$$

After the rough surface S_r being discretized along the x-axis and the target S_o being discretized on the surface, the MoM with point-matching is used. The boundary conditions are used and the matrix obtained from (1a)–(1c) as follows:

$$\begin{bmatrix} A & B & 0 \\ C & -\rho D & E \\ F & -\rho G & H \end{bmatrix} \begin{bmatrix} V_1 \\ V_2 \\ V_3 \end{bmatrix} = \begin{bmatrix} \Psi_{inc} \\ 0 \\ 0 \end{bmatrix} \tag{3}$$

where $V_1(x) = \Psi_0(\mathbf{r})\,|_{\mathbf{r}\in S_r}$, $V_2(x) = \partial\Psi_0(\mathbf{r}')/\partial n'|_{\mathbf{r}\in S_r}$, $V_3(x) = \Psi_1(\mathbf{r})\,|_{\mathbf{r}\in S_0}$. The details of A, B, C, D, E, F, G, H are given in [3]. Since the scattering field in the space above the surface is radiated from the "equivalent current on the rough surface", after solving (3), the scattering near field is calculated by substituting the known $V_1(x)$ and $V_2(x)$ into the first part of the right hand side of Equation 1(a), that is:

$$\Psi_s(\mathbf{r}) = \int_{S_r}\left[V_1(x)\,\frac{\partial \mathrm{g}_0(\mathbf{r},\mathbf{r}')}{\partial\mathbf{n}'} - \mathrm{g}_0(\mathbf{r},\mathbf{r}')V_2(x)\right]ds' \quad \mathbf{r}'\in S_r \tag{4}$$

Here, $\mathbf{r}$ represents the receivers' position.

There are hundreds of samplings both in the training data set and the testing data set, and for each sampling, Equations (3) and (4) must be calculated and solved. So it is time-consuming to generate the training and testing data sets. To save calculation time, a new fast backward and forward (FBM) method called cross coupling iterative approach (CCIA) proposed in [4] is used.

3. INVERSE PROBLEM FORMULATION

From Section 2, it can be seen that the measured scattered electric field $\mathbf{E}_{sca}$ at the observing points are closely related to the position of the PEC cylinder below the rough surface. That is

$$\mathbf{E}_{sca} = \phi(\mathbf{u}) \tag{5}$$

where $\mathbf{u}$ is the position of the scatter (xp and h), and ϕ represents the relationship between $\mathbf{u}$ and $\mathbf{E}_{sca}$.

The aim of the reconstruction is to find the unknown position of the PEC cylinder from $\mathbf{E}_{sca}$. Mathematically, this reduces to determination of the following relation [17]:

$$\mathbf{u} = \phi^{-1}\left(\mathbf{E}_{sca}\right) \tag{6}$$

This problem can be reformulated as a regression problem, where the unknown function ϕ^{-1} must be approximated from the knowledge of a number of known I/O pairs of vectors $\left\{\left(\mathbf{E}_{sca}\right)_i, \left(\mathbf{u}\right)_i\right\}$ $i = 1, 2, \ldots, N$. Once ϕ^{-1} is known, the unknown parameters of the scatter can be worked out immediately when the scatter field is measured. As a powerful tool for function regression problems, multi-output LS-SVM is used for the approximation of ϕ^{-1} in this paper.

4. MULTI-OUTPUT LS-SVM

Reference [15] gives the details of multi-output LS-SVM, and they are introduced briefly here.

Given a set of training data points $\{\mathbf{x}_i, \mathbf{y}_i\}$ $i = 1, \ldots, N$, where $\mathbf{x}_i \in R^m$ is the input data, $\mathbf{y}_i \in R^l$ the output, and N the size of training data set. Then the multi-output LS-SVM is turned to solving the following linear equation [15]:

$$\begin{bmatrix} 0 & \mathbf{1}^T \\ \mathbf{1} & \mathbf{\Omega} + \gamma^{-1}\mathbf{I} \end{bmatrix} \begin{bmatrix} \mathbf{b} \\ \boldsymbol{\alpha} \end{bmatrix} = \begin{bmatrix} \mathbf{0}^T \\ \mathbf{Y} \end{bmatrix} \tag{7}$$

$$\mathbf{Y} = [\mathbf{y}_1, \mathbf{y}_2, \ldots, \mathbf{y}_l] = \begin{bmatrix} y_{11} & \cdots & y_{1l} \\ \vdots & \ddots & \vdots \\ y_{N1} & \cdots & y_{Nl} \end{bmatrix} \tag{8a}$$

$$\boldsymbol{\alpha} = [\boldsymbol{\alpha}_1, \boldsymbol{\alpha}_2, \ldots, \boldsymbol{\alpha}_l] = \begin{bmatrix} \alpha_{11} & \cdots & \alpha_{1l} \\ \vdots & \ddots & \vdots \\ \alpha_{N1} & \cdots & \alpha_{Nl} \end{bmatrix} \tag{8b}$$

Here γ is a constant value which balance the generalization capability and the accuracy of multi-output LS-SVM; $\mathbf{1} = [1, 1, \ldots, 1]^T$ is an N-dimensional column vector, and $\mathbf{I}$ is a $N \times N$ identity matrix; $\mathbf{\Omega}_{ij} = k\left(\mathbf{x}_i, \mathbf{x}_j\right)$; $k\left(\mathbf{x}_i, \mathbf{x}_j\right)$ is the kernel function. Usually, radial basis function (RBF) $k(\mathbf{x}, \mathbf{y}) = \exp(-\frac{\|\mathbf{x}-\mathbf{y}\|^2}{2\sigma^2})$ is used as the kernel function, where σ^2 is the kernel parameter. Both σ^2 and γ need to be determined

during the training process. After trained properly, when a new input $\mathbf{x}$ is given, the corresponding output by multi-output LS-SVM is as:

$$\hat{y}_j(\mathbf{x}) = \sum_{i=1}^{N} \alpha_{ij} k(\mathbf{x}, \mathbf{x}_i) + b_j \quad (j = 1, 2, \ldots l) \tag{9}$$

5. NUMERICAL RESULTS

To validate the multi-output LS-SVM in the buried target reconstruction, several numerical simulations are shown in this section.

The tapered wave, with frequency of 1.2 GHz and tapering parameter $g = L/4$ ($L = 25.6\lambda$ is the length of the rough surface), normally incidents into the soil at the center of the surface. The rough surface uses Gaussian spectrum with a correlation length $l = \lambda$ and root mean square height $\bar{h} = 0.1\lambda$. The relative permittivity of the earth is $\epsilon_r = 4.0 + j0.01$. Since the ground is not varying, here the rough surface does not change once it is generated. The receivers are at $x_i = -5\lambda + 0.25\lambda * i$ $i = 0, 1, \ldots, 40$ on the measurement line at $\mathbf{H}= \lambda$ above the surface. The radius of the target is $R = \lambda$, and the position of the target (xp, h), which is also the center of the target, is to be reconstructed.

The data for both the training and testing sets are obtained from solving the direct scattering problem. The training set is made up by 441 examples. In particular, 21 different values of xp ($xp = -\lambda + 0.1\lambda * i$, $i = 0, 1, \ldots, 20$), 21 values of h ($h = -1.5\lambda - 0.1\lambda * i$, $i = 0, 1, \ldots, 20$) have been used. To assess the multi-output LS-SVM, the training set, made up by 121 examples, including 11 different values of xp ($xp = -0.95\lambda + 0.20\lambda * i$, $i = 0, 1, \ldots, 10$) and 11 different values of h ($h = -1.55\lambda - 0.20\lambda * i$, $i = 0, 1, \ldots, 10$)), is used.

In all the simulations, while the input data for regression are the amplitude of scattered electric field measured at the observation points, the output data are xp and h. The hyper parameters (σ^2 and γ) of multi-output LS-SVM are worked out by a very effective procedure called sequential minimal optimization (SMO) [16] during the training process. Usually, the training process is time-consuming. However, the offline training can be done. After properly trained, xp and h can be reconstructed by regression within few seconds.

The relative error is used to quantify the accuracy of the reconstruction:

$$\text{relErr}(p) = \frac{|p_{\text{true}} - p_{\text{recons}}|}{|p_{\text{true}}|} \times 100\% \tag{10}$$

where p is the considered unknown variable. Subscript true indicates

real value of the variable, and subscript recons indicates the value reconstructed by the reconstruction method

5.1. Comparison Multi-output LS-SVM with Single-output LSSVM

This subsection deals with the comparison multi-output LS-SVM with single-output LS-SVM. For the multi-output LS-SVM, only one modal is needed, and both xp and h can be reconstructed simultaneously. But for the single-output LS-SVM, two different LS-SVM modals are needed for xp and h, respectively. The simulation results are shown in Table 1 and Figs. 2 and 3.

Table 1 summarizes the performances of the multi-output LS-SVM

Table 1. Relative errors for the reconstruction of circular PEC cylinder by multi-output LS-SVM and single-output LS-SVM.

	Parameter	Training (Max)	Training (Mean)	Testing (Max)	Testing (Mean)
multi-output LS-SVM	xp (%)	1.62	0.30	7.75	1.05
	h (%)	3.62	0.85	7.2	3.53
single-output LSSVM	xp (%)	3.07	0.59	8.23	1.63
	h (%)	4.12	1.38	7.32	3.72

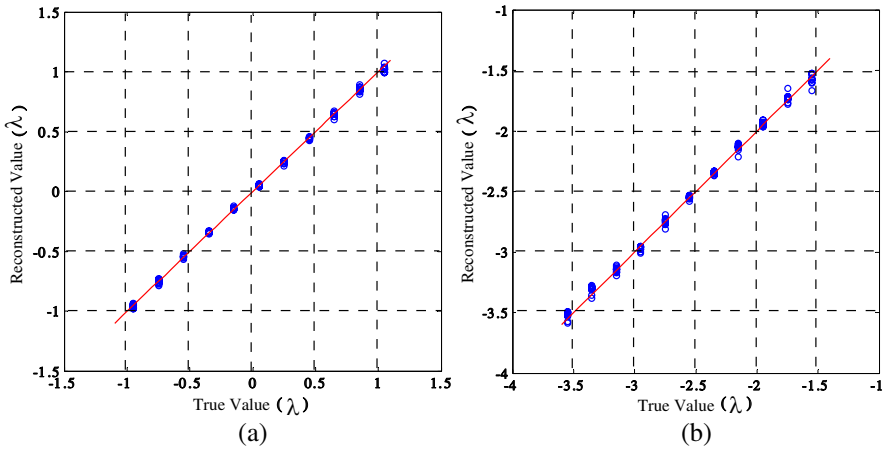

Figure 2. Position reconstruction of circular PEC cylinder by multi-output LS-SVM. (a) xp, (b) h.

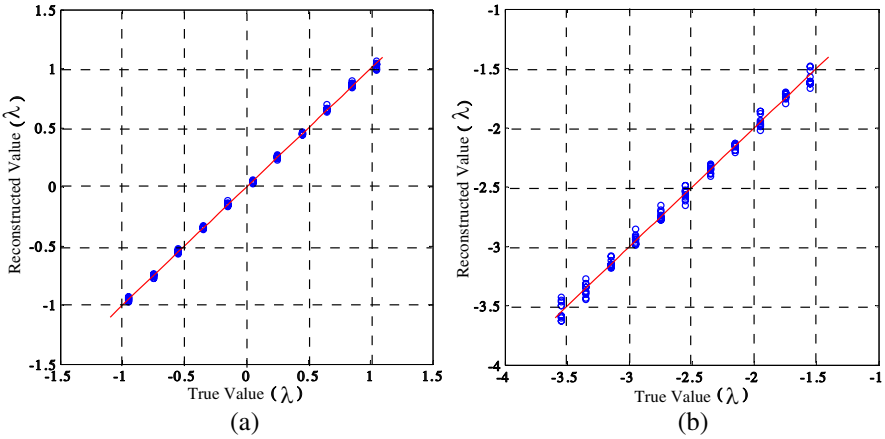

Figure 3. Position reconstruction of circular PEC cylinder by single-output LS-SVM. (a) xp, (b) h.

and single-output LS-SVM. From Table 1, it can be seen that the agreement between reconstructed values and actual ones is good, for the maximum relative errors are all below 9 percent, and the average relative errors are all less than 4% for both the testing and training data sets. Besides, the reconstruction of h is not so actually reconstructed compared with xp. Moreover, for both xp and h, multi-output LS-SVM can achieve better reconstruction than single-output LS-SVM. The reconstruction of both xp and h is illustrated in Fig. 2 and Fig. 3. The information shown by them is the same as that shown in Table 1. It can be concluded that the multi-output LS-SVM is much better than LS-SVM for buried PEC target position reconstruction.

5.2. Comparison Multi-output LS-SVM with Multi-output ANN

With the same training and testing data sets, another similar multi-output method, MLPANN, is also illustrated to compare with multi-output LS-SVM. The structure of the three layered MLPANN is 41-2020-2 (four-layer MLPANN: 41 neurons in input layer, 20 neurons in the first hidden layer, 20 neurons in the second hidden layer, and 2 neuron in output layer), and the most widely used Levenberg-Marquardt training algorithm is adopted to train MLPANN. 150 training steps are set. The reconstruction result is shown in Table 2 and Fig. 4.

Table 2. Relative errors for the reconstruction of circular PEC cylinder by multi-output LS-SVM and MLPANN.

	Para-meter	Training (Max)	Training (Mean)	Testing (Max)	Testing (Mean)
multi-output LS-SVM	xp (%)	1.62	0.30	7.75	1.05
	h (%)	3.62	0.85	7.02	3.53
multi-output MLPANN	xp (%)	6.98	1.75	9.15	3.62
	h (%)	5.21	0.82	15.06	9.87

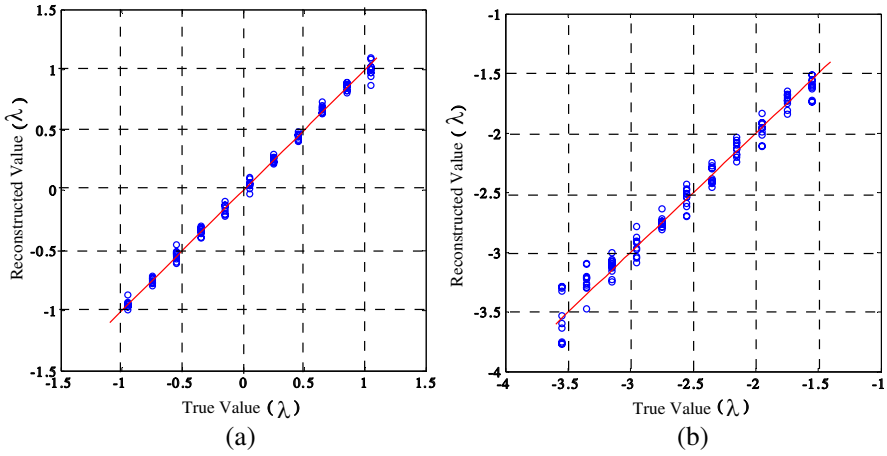

Figure 4. Position reconstruction of circular PEC cylinder by MLPNN. (a) xp, (b) h.

Table 2 summarizes the performances of the multi-output LS-SVM and MLPANN. From Table 2 for both xp and h, the reconstruction relative errors by MLPANN are much larger than that by multi-output LS-SVM, which are obvious in Fig. 4, especially when it is compared with Fig. 2. It can be concluded that the multi-output LS-SVM is much better than MLPANN for buried PEC target position reconstruction.

5.3. Robustness to Noisy Data

Generally, the data is contaminated by the noise. To make the measured data more realistic, Gaussian white noises with zero mean value and a standard deviation σ_{noise} are added to the calculated

scattered data, and σ_{noise} is given by Equation (11) [17] as follow:

$$\text{SNR} = 10\log_{10}\frac{\sum_{v=1}^{V}\sum_{m(v)=1}^{M(V)}\left|E^{v}_{scatt}(x_{m(v)}, y_{m(v)})\right|^2}{2MV\sigma^2_{\text{noise}}} \tag{11}$$

For each illumination $v = 1, \ldots, V$, the scatter field $E^{v}_{scatt}(x_{m(v)}, y_{m(v)})$ is measured at a predefined location $(x_{m(v)}, y_{m(v)})$. In this simulation $V = 1$, $M(v) = 41$, and noise with SNR = 30 dB, 25 dB, 20 dB is considered.

Table 3. Relative error analysis for position reconstruction of circular PEC cylinder by multi-output LS-SVM with different noise.

Noise level	Para-meter	Training (Max)	Training (Mean)	Testing (Max)	Testing (Mean)
30 dB	xp (%)	1.92	0.53	7.95	1.65
	h (%)	5.36	1.25	9.17	4.38
25 dB	xp (%)	2.73	0.94	8.75	2.17
	h (%)	5.92	1.83	9.82	4.66
20 dB	xp (%)	3.68	1.31	9.54	2.89
	h (%)	6.77	2.34	10.25	5.53

Table 3 summarizes the performances of the multi-output LS-SVM with different noise levels. From Table 3, it can be seen that with growing noise, for both xp and h, although the relative errors are growing, the reconstructions are still satisfying. The average relative errors are all less than 7% for the both the testing and training data sets. Therefore, to some extent, the reconstructed values agree with the corresponding actual ones. It can be concluded that the multi-output LS-SVM is noise tolerant for buried PEC target position reconstruction.

6. CONCLUSION

In this paper, the position reconstruction of the buried PEC target below rough surface is treated as a regression problem. Multi-output LS-SVM is presented as the efficient regression tool, and the training and testing date sets are generated by the amplitude of the scattering data calculated by MoM. On the one hand, it is more precise than MLPNN and single-output LS-SVM; on the other hand, it needs not to train each unknown like SVM or single-output LS-SVM. The

simulation results show that even the data are added with 20 dB Gaussian white noise, the multi-output LS-SVM can still reconstruct the target in the right position. It can be concluded that the multi-output LS-SVM to the position reconstruction of buried PEC target below rough surface is valid.

ACKNOWLEDGMENT

This work was supported by the National Key Laboratory of Millimeter Waves at Southeast University in China (No. K201201); the Natural Science Foundation of Shanxi Province, China (No. 2011JM8025).

REFERENCES

1. Bermani, E., S. Caorsi, and M. Raffetto, "An inverse scattering approach based on a neural network technique for the detection of dielectric cylinders buried in a lossy half space," *Progress In Electromagnetics Research*, Vol. 26, 67–87, 2000.
2. Li, F. H., Q. H. Liu, and L. P. Song, "Three-dimensional reconstruction of objects buried in layered media using born and distorted born iterative methods," *IEEE Trans. on Geoscience and Remote Sensing Letters*, Vo. 1, No. 2, 107–111, 2004.
3. Wang, X., C.-F. Wang, and Y.-B. Gan, "Electromagnetic scattering from a circular target above or below rough surface," *Progress In Electromagnetics Research*, Vol. 40, 207–227, 2003.
4. Ji, W. J., C. M. Tong, and P. W. Yan, "Fast calculation of EM scattering from randomly rough surface with buried PEC target," *Chinese Journal of Radio Science*, Vol. 24, No. 5, 939–965, 2009.
5. Firoozabadi, R., E. L. Miller, and C. M. Rappaport, "New inverse method for simultaneous reconstruction of object buried beneath rough ground and the ground surface structure using SAMM forward model," *Proceedings of SPIE*, Vol. 5674, 382–393, 2005.
6. Cai, J. L., Z. Bao, C. M. Tong, et al., "Inversion of PEC targets below dielectric rough surface based on hybrid multi-phase particle swarm optimization," *System Engineering and Electronics*, Vol. 34, No. 12, 2433–2437, 2012.
7. Cmielewski, O., H. Tortel, and A. Litman, "A two-step procedure for characterizing obstacles under a rough surface from bistatic measurements," *IEEE Trans. on Geoscience and Remote Sensing*, Vol. 45, No. 9, 2850–2858, September 2007.
8. Altuncu, Y., O. Ozdemir, and I. Akduman, "Imaging of dielectric objects buried under an arbitrary rough surface,"

IEEE International Geoscience and Remote Sensing Symposium, IGARSS, 2954–2957, 2006.

9. Vapnik, V. N., *The Nature of Statistical Learning Theory*, 2nd Edition, Springer-Verlag, New York, 1995.
10. Bermani, E., A. Boni, S. Caorsi, and A. Massa, "An innovative real-time technique for buried object detection," *IEEE Transactions on Geoscience and Remote Sensing*, Vol. 41, No. 4, 927–931, 2003.
11. Wu, H. B., J. J. Yao, and S. Y. He, "Parameters extraction of the two-dimensional object above or on a rough surface based on the electromagnetic simulation," *Journal of Wuhan University*, Natural Science Edition, Vol. 55, No. 6, 705–709, 2009.
12. Bermani, E., A. Boni, A. Kerhet, and A. Massa, "Kernal evaluation of SVM based estimation for inverse scattering problems," *Progress In Electromagnetics Research*, Vol. 53, 167–188, 2005.
13. Wang, F. F. and Y. R. Zhang, "The support vector machine for dielectric target detection through a wall," *Progress In Electromagnetics Research Letters*, Vol. 23, 119–128, 2011.
14. Zhang, Q. H., B. X. Xiao, and G. Q. Zhu, "Inverse scattering by dielectric circular cylinder using support vector machine approach," *Microwave and Optical Technology Letters*, Vol. 49, No. 2, 372–375, 2007.
15. Cai, J. L., C. M. Tong, and W. J. Zhong, "Reconstruction of dielectric cylinder by multi-output least square support vector machine," *Cross Straight Quad-region Radio Science and Wireless Technology Conference (CSQRWC)*, Vol. 1, 160–163, 2011.
16. Platt, J., *Fast Training of Support Vector Machines Using Sequential Minimal Optimization, Advances in Kernel Methods-support Vector Learning*, MIT Press, Cambridge, MA, 1999.
17. Donelli, M. and A. Massa, "Computational approach based on a particle swarm optimization for microwave imaging of two dimensional dielectric scatters," *IEEE trans. on Microwave Theory and Techniques*, Vol. 53, No. 5, 1761–1776, 2005.